Bio-Inspired Supramolecular Hybrid Dendrimers Self-Assembled from Low-Generation Peptide Dendrons for Highly Efficient Gene Delivery and Biological Tracking

Xianghui Xu, Yeting Jian, Yunkun Li, Xiao Zhang, Zhaoxu Tu, and Zhongwei Gu*

National Engineering Research Center for Biomaterials, Sichuan University, Chengdu, Sichuan 610064, P.R. China

ABSTRACT Currently, supramolecular self-assembly of dendrons and dendrimers emerges as a powerful and challenging strategy for developing sophisticated nanostructures with excellent performances. Here we report a supramolecular hybrid strategy to fabricate a bio-inspired dendritic system as a versatile delivery nanoplatform. With a rational design, dual-functionalized low-generation peptide dendrons (PDs) self-assemble onto inorganic nanoparticles *via* coordination interactions to generate multifunctional supramolecular hybrid dendrimers (SHDs). These SHDs exhibit well-defined nanostructure, arginine-rich peptide corona, and fluorescent signaling properties. As expected, our bio-inspired supramolecular hybrid strategy largely enhances the gene transfection efficiency of SHDs approximately 50 000-fold as compared to single PDs at the same R/P ratio. Meanwhile the bio-inspired SHDs also (i) provide low cytotoxicity and serum resistance in gene delivery; (ii) provide inherent fluorescence for tracking intracellular pathways including cellular uptake, endosomal escape, and gene release; and (iii) work as an alternative reference for monitoring desired protein expression. More importantly, *in vivo* animal experiments demonstrate that SHDs offer considerable gene transfection efficiency (in muscular tissue and in HepG2 tumor xenografts) and real-time bioimaging capabilities. These SHDs will likely stimulate studies on bio-inspired supramolecular hybrid dendritic systems for biomedical applications both *in vitro* and *in vivo*.

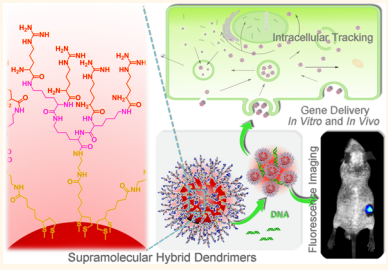

KEYWORDS: bio-inspired nanomaterials · supramolecular hybrid dendrimers · peptide dendrons · gene delivery · biological tracking

Development of molecular nanomaterials (*e.g.*, polymer and dendrimer) and supramolecular nanomaterials (*e.g.*, liposome, micelle, and polymersome) with well-defined nanostructures and advanced functions has made a significant impact on biomedicine, particularly in the field of therapeutic agent delivery.[1,2] Notably, dendrimers are widely regarded as inherent and versatile nanocarriers for therapeutic agent delivery, owing to their unique properties such as perfectly monodisperse chemical structure and highly branched three-dimensional architecture.[3,4] However, dendrimer-based nanocarriers are now likely to meet some practical problems on their extensive biomedical applications.[5] First, it is very difficult to manufacture high-generation dendrimers as compared to other macromolecules; therefore, high cost largely hinders their industrialization and commercialization. Second, high-generation dendrimers possess much higher delivery efficiency but usually coincide with more serious toxicity to targeted cells than low-generation dendrimers.[6] Currently, new chemical approaches are explored to resolve these conflicts and difficulties in biomedical applications of dendrimer-based nanocarriers. On one hand, cross-linking low-generation poly(amido amine) (PAMAM) dendrimers *via* bioreducible covalent bonds has generated some efficient and biocompatible nanocarriers which are obviously superior to classic high-generation dendrimers.[7,8] On the other hand, in recent years, self-assembly of dendrimers and dendrons *via* noncovalent interactions has attracted significant attention from researchers in chemistry and materials science to construct supramolecular dendritic systems

* Address correspondence to zwgu@scu.edu.cn.

Received for review June 9, 2014 and accepted September 3, 2014.

Published online September 03, 2014
10.1021/nn503118f

mimicking natural sophisticated nanostructures with excellent performance.[9,10]

Especially in the biomedical field, self-assembling amphiphilic dendrons and dendrimers into supramolecular dendritic systems is the most promising chemical strategy to generate the latest delivery nanoplatforms,[11,12] which have held great potential for the therapeutic delivery of drugs,[13−15] genes,[16−18] vaccines,[19] and molecular probes.[20] Recently, we also reported some strategies on supramolecular self-assembly of peptide dendrimers into bio-inspired nanostructures for efficient drug and gene delivery.[21,22] However, until now, supramolecular dendritic systems as carriers for mechanistic studies and *in vivo* delivery have only shown limited success, similar to other artificial vehicles.[23,24] Toward the goal of ideal delivery platforms, the existing supramolecular dendritic systems now urgently need to be equipped with more advanced features such as high delivery efficacy both *in vitro* and *in vivo*, good biocompatibility, multifunctionality, facile manufacture, and low cost. More importantly, new supramolecular dendritic systems are expected to gain more insights into the delivery mechanism and address *in vivo* issues. As a result, challenges and opportunites for fabricating supramolecular dendritic systems as versatile platforms for highly efficient delivery remain. Additional chemical strategies are able to develop new supramolecular dendrimer systems for in-depth studies.[25]

Besides natural supramolecular architecture and performance, natural systems provide other numerous bio-inspirations to improve artificial delivery systems, such as hierarchical structure, sophistication, hybridization, and multifunctionality.[26,27] For example, some of the latest attempts at mimicking key features of natural carriers (*e.g.*, virus and bacteria) largely improve maximal therapeutic efficacy with minimal side effects.[25,26,28,29] In this regard, peptide dendrons and dendrimers should be one of the most suitable blocks for bio-inspired nanofabrication because they have many inherent properties to mimic natural proteins such as components, morphology, and bioactivity.[9,10,30] Another current focus concerns the simulation of natural hybrid materials to obtain many hybrid nanoobjects, which combine certain beneficial properties of the inorganic and organic components to generate multifunctional nanoplatforms.[31,32] Above-mentioned lessons motivated us to develop a novel bio-inspired supramolecular dendritic system with a rational chemical design and validate its utility in biomedicine.

A major advancement of this work is a novel strategy to generate efficient and biocompatible supramolecular hybrid dendrimers (SHDs) which incorporated some bio-inspirations to achieve the following features: (i) hierarchical nanostructures with a dendritic peptide corona and an inorganic core to simulate the sophisticated nanostructures in nature, (ii) self-assembled arginine-rich surfaces to mimic the components of cell-penetrating peptides for enhancing internalization and endosomal escape,[33,34] (iii) inherent hybrid properties (*e.g.*, fluorescence property and high electron contrast) for intracellular tracking by optical microscopy and electron microscopy to elucidate the delivery pathway, and (iv) high gene delivery efficiency to explore the *in vivo* utility of the supramolecular dendritic system. To the best of our knowledge, SHDs are the first demonstration of bio-inspired supramolecular dendritic systems for efficient gene delivery and biological tracking *in vitro* and *in vivo*.

RESULTS AND DISCUSSION

To prove our idea, dual-functionalized low-generation peptide dendrons (PDs) were designed for supramolecular hybrid self-assembly (Figure 1A). The PD peripheral groups were completely functionalized with arginine; their cores were modified with lipoic acid (LA) with coordinating potentials. In this supramolecular hybrid design, inorganic nanoparticles were used as templates because their accessible surfaces could provide coordination sites for the self-assembly of PDs and their unique properties could enrich the functionalities of new supramolecular dendritic systems such as iron oxide nanoparticles for magnetic resonance imaging, quantum dots (QDs) for fluorescence imaging, and gold nanoparticles for near-infrared absorption.[31,32] QDs were used as model templates due to their fluorescent properties for both *in vitro* detection and *in vivo* fluorescence imaging.[35,36] Inspired by some recent studies on aqueous phase transfer, we adopted a convenient and efficient approach through UV irradiation (λ = 365 nm) to realize *in situ* reduction of the LA groups (functionalized core of PDs) into dihydrolipoic acid (DHLA).[37,38] Then the dual-functionalized PDs could spontaneously coordinate onto the surface of QDs to generate a single bio-inspired SHD (Figure 1B). The preparation details of SHDs are described in the Supporting Information (Figure S5). We believe that SHDs not only provide supramolecular hybrid properties for efficient gene delivery and inherent fluorescence for biological tracking *in vitro* but also offer significant potentials to high gene transfection efficiency and distinct bioimaging *in vivo* (Figure 1C).

First, the dual-functionalized low-generation PDs were obtained with precise molecular structure and excellent water solubility. The molecular weight of PDs detected by matrix-assisted laser desorption ionization time-of-flight mass spectroscopy (MALDI-TOF MS) agreed very well with its theoretical value (Figure 2A). The detailed synthetic procedures and characterizations of the dual-functionalized PDs can be found in the Supporting Information.

With *in situ* reduction of PDs *via* UV irradiation, supramolecular coordination interactions spontaneously drove the formation of SHDs. ^{1}H NMR results

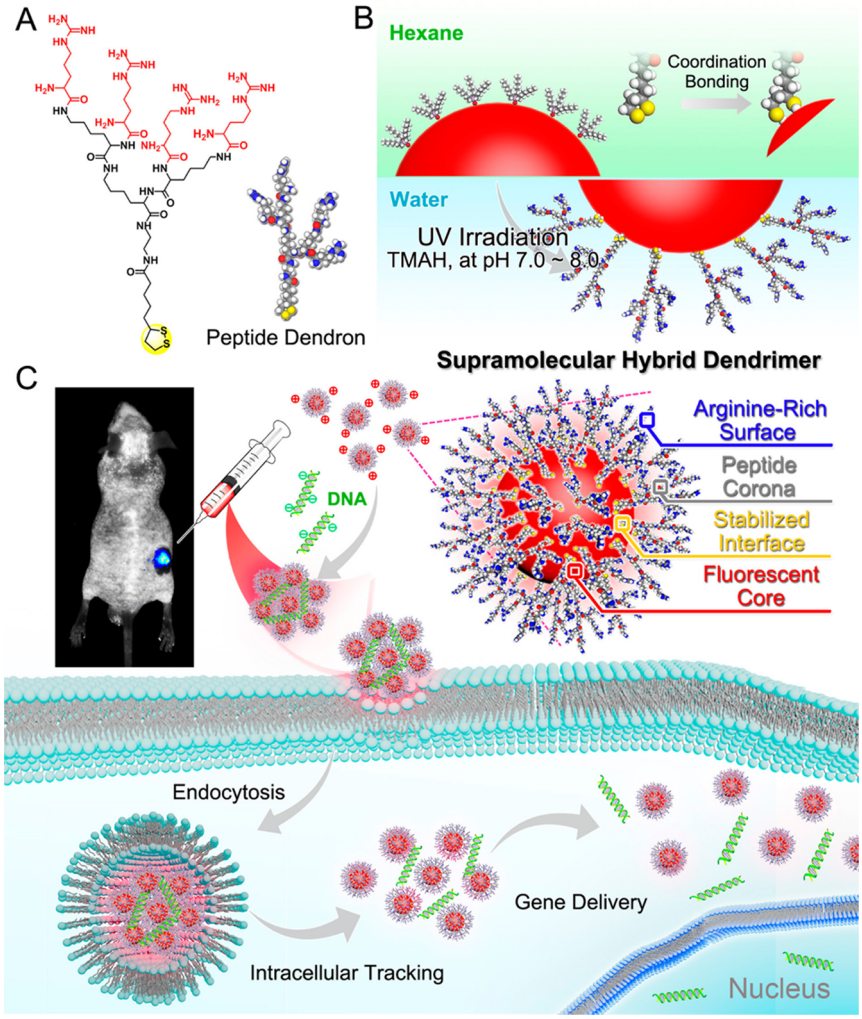

Figure 1. Schematic illustrations for self-assembly and biomedical applications of SHDs. (A) Chemical structure of the dual-functionalized PDs, (B) self-assembly of PDs onto quantum dots *via* coordination interactions, and (C) SHDs with hierarchical nanostructures for gene delivery and biological tracking *in vitro* and *in vivo*.

showed that all signals of PDs clearly appeared in the spectrum of SHDs, and this result coupled with fluorescent images indicated that the dual-functionalized PDs successfully self-assembled into SHDs with fluorescent properties (Supporting Information Figure S6). Inspection of the FT-IR spectra showed that SHDs obtained a distinct peak ($\nu_{C=O}$, 1669 cm^{-1}) from the supramolecular dendritic peptide corona (Figure S7). As shown in Figure 2B, thermogravimetric analysis (TGA) curves revealed that the presence of PDs in SHDs was 40.51 wt %. It was indicated that hundreds of PDs self-assembled into a single SHD, and eight peripheral groups on low-generation PDs were amplified to thousands of peripheral groups on the surface of SHDs by virtue of supramolecular effects.

As shown by transmission electron microscopy (TEM), SHDs presented a well-defined spherical shape of approximately 8 nm diameter, which agreed with an average size of 7.96 ± 0.93 nm by dynamic light scattering (DLS) measurement (Figure 2C). The zeta-potential of SHDs was 17.3 ± 0.4 mV. The scanning electron microscopy (SEM), energy-dispersive spectroscopy (EDS), and atomic force microscopy (AFM) data further confirmed the component and structure of SHDs (Figure S10). Fluorescence images and spectra demonstrated that SHDs had excellent water solubility and fluorescence characteristics (Figure 2D). When we inspected the stability of SHDs, size distribution and fluorescence intensity were not notably altered in aqueous solution for a long time (Figure S13 and Figure S14). Compared to some previous supramolecular dendritic systems which were mainly based on hydrophobic effects for a single application,[13−22] these SHDs have better stability and more functionalities owing to the stronger noncovalent interactions and rational hybridization, which are urgently pursued for current supramolecular nanomaterials.[39,40] Moreover, this approach can be easily extended to engineer more types of supramolecular hybrid dendrimers composed of various organic dendrons and inorganic cores.

Once we confirmed the formation of SHDs, we next studied their utility for gene delivery. The binding

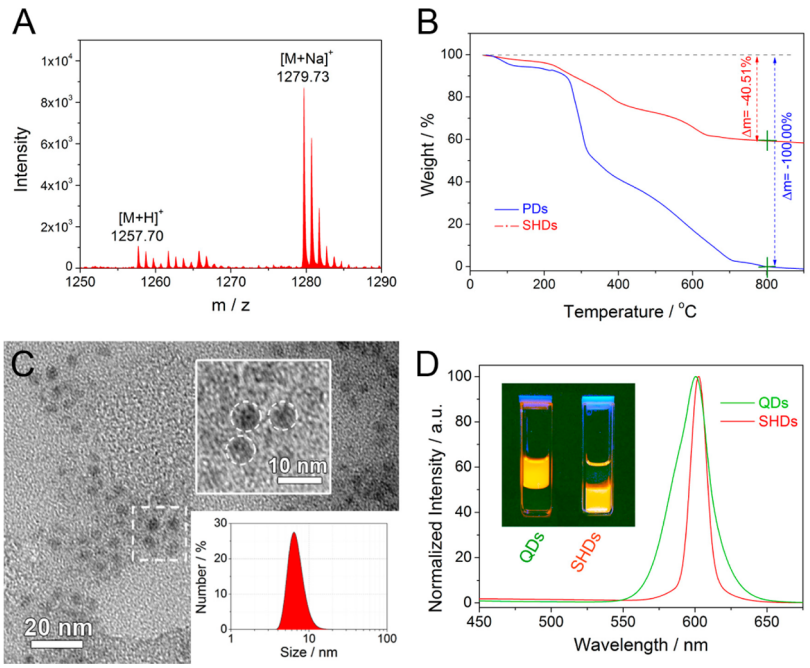

Figure 2. (A) MALDI-TOF mass spectrum of the dual-functionalized PDs. MS (*m/z*, $[M + H]^+$): 1257.70 (observed), 1257.80 (calculated). MS (*m/z*, $[M + Na]^+$): 1279.73 (observed), 1279.78 (calculated). (B) TGA curves of PDs and SHDs under flowing air with a ramp rate of 10 °C min^{-1}. (C) TEM image and DLS result (in aqueous solutions) of SHDs. (D) Fluorescence image of QDs and SHDs in *n*-hexane phase (top) and aqueous phase (bottom) and fluorescence spectra of QDs (in *n*-hexane) and SHDs (in aqueous solutions).

ability of SHDs with DNA was determined by agarose gel retention assay. The fluorescent images showed that the SHDs with red fluorescence had appropriate DNA binding ability. In Figure 3A, the R/P is the molar ratio of arginine (R) in SHDs to DNA phosphate groups (P). The DNA mobility in the SHD/DNA complex was completely retarded at the R/P ratio of 10. The TEM, SEM, and AFM results consistently suggested that the positively charged SHDs and the negatively charged DNA could assemble into compact nanoparticles with an average size of 143.33 ± 8.79 nm in aqueous solution (Figure 3B and Figures S16 and S17).

Next, quantitative results of pGL3-Luc delivery efficiency in a human hepatocellular carcinoma HepG2 cell line proved that the bio-inspired supramolecular strategy could construct highly efficient gene vehicles using the low-generation PDs (Figure 3C). First, supramolecular effects largely enhanced the transfection efficiency of pGL3-Luc approximately 50 000-fold as compared to single PDs at the same R/P ratio of 20. Second, in the culture medium containing 10% fetal bovine serum (FBS), luciferase gene transfection mediated by SHDs (R/P 20) was much more efficient than that mediated by polyethylenimine (PEI). Additionally, the luciferase activity of the SHD group with FBS was still about 30-fold higher than that of the PEI/pGL3 complex without FBS, which is widely regarded as a gold standard for nonviral vectors. These advantages (*e.g.*, strong DNA binding ability, high efficiency, and serum resistance) of SHDs should be attributed to the dendritic peptide coronas with self-assembled arginine-rich surfaces which mimic some structures and components of viral capsids.[25,26,29,33,34]

Cytotoxicity is an important consideration for gene carriers. Thus, SHDs were evaluated for cell viability and cell apoptosis *via* cell counting kit-8 (CCK-8) assay and the propidium iodide (PI) apoptosis assay, respectively. The SHDs have no obvious cytotoxicity to HepG2 cells at a range of R/P 2.5 to R/P 20, while the PEI/DNA group caused significant cytotoxicity (~50% cell viability) due to the native drawback of cationic polymers (Figure 3D). At the same time, the number of apoptotic cells in the PEI group was nearly three times higher than that of the control group and the SHD group (Figure 3E). Collectively, this bio-inspired design gives remarkable effects to SHDs for gene delivery, including high efficiency, serum resistance, and low cytotoxicity.

A better understanding of gene delivery mechanisms such as cellular uptake, intracellular traffic, and endosomal escape is important for improving gene delivery systems of even typical gene vectors (*e.g.*, lipid-based nanoparticle).[41] Another important goal of our chemical design is to present a preliminary delivery pathway of the latest supramolecular dendritic systems, which can be studied *via* their inherent fluorescence and high electron contrast. We combined quantitative fluorescent sorting, fluorescent microscopy, and electron microscopy to explore the intracellular fate of the SHD/DNA complex in HepG2 cells.

Confocal laser scanning microscopy (CLSM) images coupled with fluorescence-activated cell sorting (FACS) analysis showed that the SHD/DNA complex attached onto the cell membrane and internalized into HepG2 cells within a short time (Figure 4A and Figure S19, SHDs with red fluorescent signals and Cy5-labeled DNA

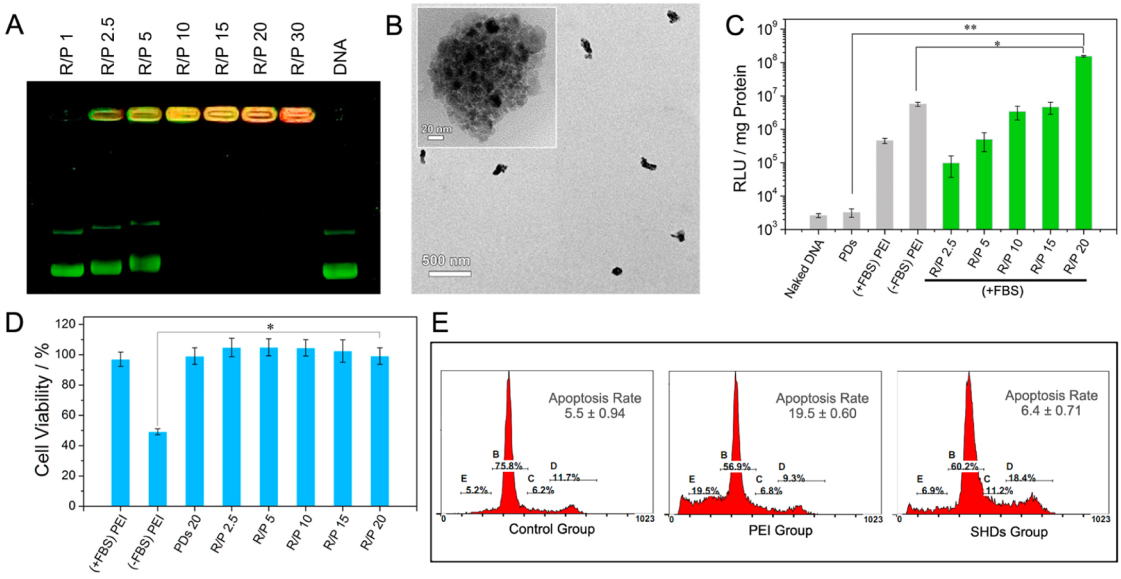

Figure 3. (A) Merged fluorescence image of the SHD/DNA complex by gel electrophoresis assay including red fluorescent SHDs and green fluorescent DNA. (B) TEM image of the SHD/DNA complex and a magnified TEM image for a single SHD/DNA complex. (C) Luciferase activity in HepG2 cells after exposure to the SHD/pGL3 complex at various R/P ratios for 48 h (*$p < 0.01$, **$p < 0.001$, mean ± SD, $n = 6$). (D) Viability of HepG2 cells after exposure to the PEI/DNA complex (N/P 10), PDs/DNA complex (R/P 20), and the SHD/DNA complex (R/P from 2.5 to 20) for 48 h (mean ± SD, $n = 6$). (E) Apoptosis of HepG2 cells after incubation with the PEI/DNA complex (N/P 10) and the SHD/DNA complex (R/P 20) for 48 h (mean ± SD, $n = 6$).

with green fluorescent signals). After exposure to the SHD/DNA complex for 3 h, the SHD/DNA complex was entrapped by organelles such as endosomes and lysosomes (overlap of red fluorescence, green fluorescence, and blue fluorescence). Encouragingly, the majority of the SHDs and DNA could escape from endosomes at 8 h. Indeed, most DNA was released from the SHD/DNA complex into the cytosol within 8 h (dissociation of red fluorescence, green fluorescence, and blue fluorescence). Eventually, DNA was mainly scattered across the perinuclear region with delivery into the nucleus to exert gene transfection within 18 h.

To illustrate this process more intuitively, live cell imaging system (LCIS) was used to track intracellular pathways in HepG2 cells in real time (Figure 4B). We showed that (1) the SHD/DNA complex was actively transported into the cell and collectively accumulated into the endocytic compartments (Figure S20 and supporting video 1), (2) the complex moved toward nucleus (Figure S21 and supporting video 2) and (3) went around the nucleus within 4 h (Figure S22 and supporting video 3). We then ascertained the subcellular location of the complex using TEM. As shown in Figure 4C, some of SHD/DNA complex was internalized by endocytosis from an extracellular matrix. More complex was clearly found in the multivesicular structures of endosomes and lysosomes, and part of the complex was distributed in the cytosol.

Current research indicates that successful gene delivery ultimately depends on whether the gene delivery vectors could serve as a natural virus to overcome the biological barriers such as biodegradation, cellular uptake, and nuclear delivery.[25,29,42] Overall, these results collectively suggest that SHDs successfully conquered several biological obstacles and mimicked some key progresses of viruses infection for gene delivery (Figure 4D): (i) packaging and protecting nucleic acid, (ii) achieving a rapid internalization, (iii) facilitating the endosomal escape, and (iv) delivering DNA to the perinuclear region for high protein expressions.

The ultimate goal of delivery vehicles is high gene translation of the desired protein. Fortunately, our design also gives the SHD fluorescence for quantitative analysis and offers a deeper understanding of the relationship of SHDs and the desired protein expression (Figure S23 and Figure S24). Gene delivery of the SHD/pEGFP complex illustrated that the complex was internalized into ~75% of HepG2 cells at 12 h; meanwhile, only a small number of cells (~15%) expressed green fluorescent protein (GFP) (Figure 5A). In addition, mean fluorescence intensity (MFI) of GFP was much lower than that of SHDs (Figure 5B). After 12 h, the percentage of SHD-positive cells and MFI (SHDs) remained stable up to 60 h. Significantly, the percentage of GFP-positive cells and MFI (GFP) increased more than 3- and 5-fold, respectively. Intracellular tracking suggested that the pEGFP was translated into proteins efficiently after delivery to perinuclear locations. These findings perfected the above-mentioned intracellular tracking of the gene delivery process. Subsequently, with the same concentration of pEGFP in each group, we found that the amount of protein expression greatly depends on the SHDs. Higher gene transfection efficiency was seen with increased SHD internalization (Figure 5C,D). Thus, the success of the bio-inspired

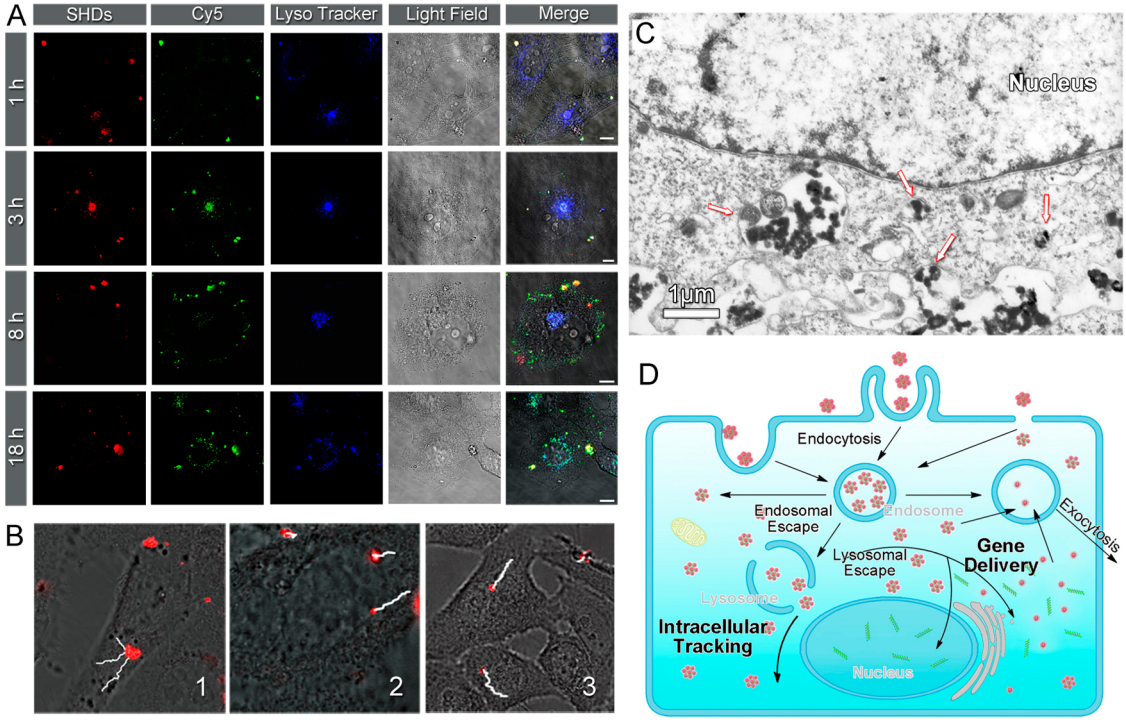

Figure 4. (A) CLSM images for intracellular tracking of the SHD/DNA complex at different time points including SHD channel (red), Cy5-labeled DNA channel (green), LysoTracker-stained lysosome channel (blue), light image, and overlay of previous images. The scale bars correspond to 10 μm. (B) LCIS observation for intracellular trafficking of the SHD/DNA complex; white lines for motion trails of the SHD/DNA complex in HepG2 cells. (C) TEM image for subcellular location of the SHD/DNA complex in HepG2 cell. (D) Schematic diagram of intracellular gene delivery mediated by SHDs.

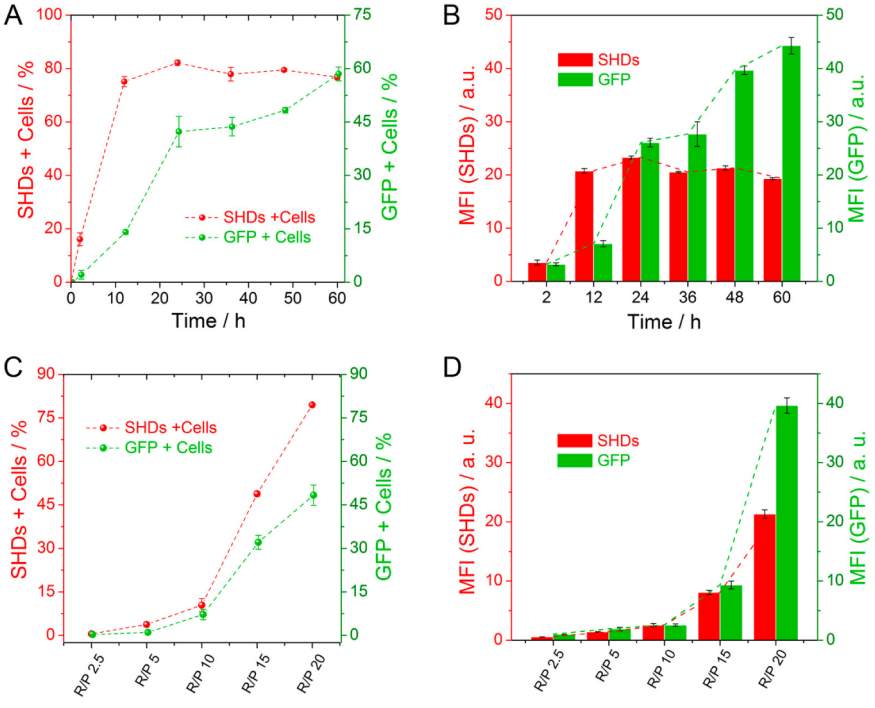

Figure 5. (A) Percentage of SHD-positive cells and GFP-positive cells at different time points as detected by FACS (R/P 20). (B) MFI (SHDs) and MFI (GFP) at different points in time (R/P 20) detected by FACS. (C) Percentage of SHD-positive cells and GFP-positive cells with different R/P ratios for 48 h detected by FACS. (D) MFI (SHDs) and MFI (GFP) with different R/P ratios after 48 h and detected by FACS.

supramolecular strategy for highly efficient gene delivery and biological tracking was fully verified.

Encouraged by this excellent performance, *in vivo* gene delivery and imaging were further carried out to

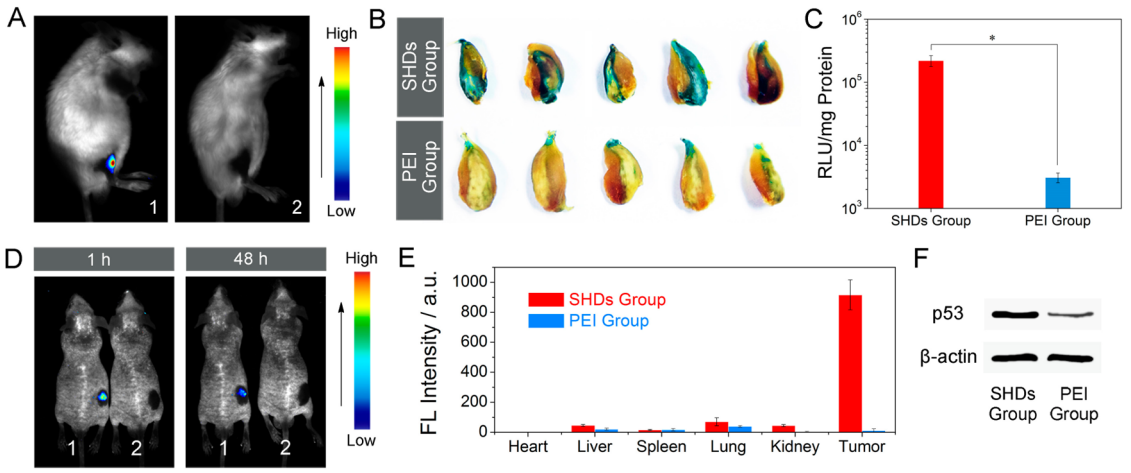

Figure 6. (A) Fluorescence images of BALB/c mice for the SHD group (1) and the PEI group (2). (B) Transfection efficacy of pCMV-β-gal in mouse muscles after intramuscular injection for 4 days (n = 5). (C) Transfection efficacy of pGL3-Luc in mouse muscles after intramuscular injection for 4 days (n = 5, *p < 0.001). (D) Fluorescence images of nude mice bearing HepG2 tumor xenografts at 1 and 48 h after intratumoral injection for the SHD group (1) and the PEI group (2). (E) *Ex vivo* fluorescence intensity of organs after intratumoral injection for 48 h. (F) Western blot analysis for p53 protein expression in the tumor.

confirm whether SHDs still worked under *in vivo* conditions. After intramuscular injection of the SHD/DNA complex, the fluorescence signal of SHDs was clearly seen with *in vivo* bioimaging (Figure 6A). The *in vivo* gene transfection of pCMV-β-gal and pGL3-Luc was determined by β-galactosidase expression and luciferase assays.[43] As shown in Figure 6B, large dark blue domains distinctly appeared in muscular tissue because of the high β-galactosidase expression in the SHD group (R/P 20). Hardly any blue signal was seen in the PEI group. The quantitative results of luciferase activity showed that SHDs yielded optimal gene transfection of pGL3-Luc (2.2×10^5 RLU/mg of protein, R/P 20), and the PEI group produced only 3.1×10^3 RLU/mg of protein (Figure 6C). The *in vivo* transfection efficacy of luciferase activity by SHDs was over 70-fold higher than that of PEI.

To explore the preliminary theranostic applications for cancer therapy, we also investigated the intratumoral efficiency of SHDs for functional gene transfection and bioimaging. Monitoring the whole process of gene delivery found that the fluorescence signal was only observed in tumor tissues during 1 to 48 h (Figure 6D and Figure S25). The *ex vivo* fluorescence images and semiquantitative fluorescence intensity of organs also indicate that almost all of SHDs were located in tumor tissue (Figure 6E and Figure S26). More importantly, the expression of the p53 protein was tested using Western blot analysis after pCMV-p53 transfection. A relatively high expression of p53 protein which plays an important role in tumor suppression was detected in the HepG2 tumor xenografts of the SHD group *versus* the PEI control (Figure 6F).[44] Therefore, we conclude that the SHDs will be the most supramolecular dendritic system candidates for *in vivo* work. Of course, more continued studies are needed to optimize the system including integrating various therapeutic agents, achieving multimodal imaging for biological tracking, and introducing targeting and polyethylene glycol.

CONCLUSIONS

In conclusion, we have demonstrated a bio-inspired strategy to develop a supramolecular dendritic system as an analytical and efficient delivery platform. This strategy provides a novel supramolecular hybrid dendrimer with well-defined, hierarchical, and stable nanostructure *via* coordination interactions. This supramolecular strategy self-assembles low-generation PDs, generating highly efficient gene delivery efficiency *in vitro* and *in vivo* owing to the arginine-rich surface of the dendritic−peptide coronas mimicking viral capsids. This hybrid strategy gives some unique features to SHDs for intracellular tracking, protein expression monitoring, and *in vivo* bioimaging, which contribute to the comprehensive understanding of gene delivery pathways and the improvement of delivery systems. This supramolecular dendritic system was equipped with most of the essential functionalities of advanced delivery platforms such as efficient delivery, mechanistic studies, and *in vivo* work. We foresee that this work will open a new avenue for the design of more multifunctional supramolecular hybrid dendrimers and additional biomedical applications.

MATERIALS AND METHODS

Materials. H-Lys-OMe·HCl, Boc-Lys(Boc)-OH, Boc-Arg(Pbf)-OH, EDC, HBTU, PyBOP, and HOBT were purchased from GL Biochem (Shanghai, China). Lipoic acid (LA), *N*-(*tert*-butoxycarbonyl) ethylenediamine, and tetramethylammonium (TMAH) were obtained from Aladdin Reagents Company

(Shanghai, China). CdSe/ZnS QDs-605 (8.0 μM, 7.5 mg/mL) were purchased from Wuhan Jiayuan Quantum Dots Co., Ltd. (Wuhan, China). Polyethylenimine 25k (PEI, Sigma-Aldrich, USA), cell counting kit-8 (CCK-8 kit, Dojindo Laboratories, Japan), phosphate buffer solution (PBS, Sigma-Aldrich, USA), cell cycle and apoptosis analysis kit (Beyotime Institute of Biotechnology, China), and bicinchoninic acid (BCA, Pierce, USA) were obtained LysoTracker Blue DND-22 (Invitrogen, USA), and IT Cy5 nucleic acid labeling kit (Mirus Bio LLC, USA) was obtained for biological assessment. Plasmids pEGFP-C1 (Clontech, USA), pGL3-Luc (Promega, USA), pCMV-β-gal (Clontech, USA), and pCMV-p53 (Clontech, USA) were obtained with the EndoFree plasmid kit from Qiagen (Germany). Cell culture media Dulbecco's minimal essential medium (DMEM), penicillin, streptomycin, and FBS were purchased from Hyclone (USA).

Synthesis of Dual-Functionalized PDs. PD backbone was synthesized by condensation reaction of H-Lys-OMe·HCl (1.0 g, 6.2 mmol) and Boc-Lys(Boc)-OH (6.5 g, 18.7 mmol) with EDC (3.6 g, 18.7 mmol), HOBT (2.5 g, 18.7 mmol), and DIPEA (8.1 mL, 49.6 mmol) in 40 mL of CH_2Cl_2 for 24 h under a nitrogen atmosphere. After removal of *N-tert*-butoxycarbonyl groups, all peripheral groups of PDs (1.5 g, 3.6 mmol) were functionalized with Boc-Arg(Pbf)-OH (11.4 g, 21.6 mmol). Then the core of arginine-functionalized PDs (3.2 g, 1.3 mmol) was modified with LA derivative (0.4 g, 1.6 mmol). Each crude product should be purified with washing and column chromatography to obtain pure compounds. Arginine residues (guanidine groups) on PDs could be exposed by trifluoroacetic acid to generate dual-functionalized PDs. The detailed synthetic routes of PDs are described in the Supporting Information. Each compound was confirmed by ^{1}H NMR (400 MHz) and MALDI-TOF MS, which could be found in Supporting Information.

Self-Assembly of PDs into SHDs. The dual-functionalized PDs (100.0 mg) were dissolved in 5.0 mL of deionized water in a glass vial, and TMAH was used to adjust the mild alkaline conditions (pH 7−8). Then *n*-hexane solution containing QDs (1.6 μmol/L, 5.0 mL) was added into the vial under vigorous stirring, and this reaction system was placed in the UV reactor with UV irradiation (λ = 365 nm). When *in situ* reduction of LA groups into DHLA was realized in the core of PDs, these PDs would spontaneously self-assemble onto QDs *via* coordination interactions (Figure 1B). With PDs coordinated onto QDs, the generated SHDs were gradually generated and completely transferred into a water phase (Figure S5). At the end of coordination self-assembly, the *n*-hexane phase was removed under dark conditions. SHDs in aqueous solution were purified by precipitation (alcohol) and centrifugation (10 000 rpm) several times to remove excess ligands and other byproducts. Finally, the SHDs were dialyzed by a dialysis bag (MWCO 2000) in 2.0 L of deionized water in the dark for further purification, and the SHDs were obtained as light red powder after freeze-drying.

Physicochemical Characterizations. ^{1}H NMR spectra of PDs and SHDs were detected by a NMR spectrometer (Bruker Avance II, Germany) at 400 MHz in DMSO-d_6. FT-IR spectra of PDs and SHDs were recorded by a FT-IR PE spectrometer using the KBr pellet technique with a wavenumber range of 500−4000 cm^{-1}. Thermal gravimetric analysis (Netzsch STA449C, Germany) was used to confirm the composition of SHDs under flowing air with a ramp rate of 10 °C min^{-1}. The size and zeta-potential of SHDs were determined by a dynamic light scattering (Malvern NANO ZS, England) at 25 °C. The morphology of SHDs was observed by a transmission electron microscopy (FEI Tecnai GF20S-TWIN, USA). The fluorescence properties of SHDs and QDs were studied by a fluorescence spectrophotometer (Hitachi F-7000, Japan). Other physicochemical characterizations and results such as UV−vis spectra, scanning electron microscopy/energy-dispersive X-ray spectroscopy (SEM-EDS, Hitachi JSM-5900LV, Japan), and atomic force microscope (Asylum MFP-3D-BIO, USA) can be found in Supporting Information.

Preparation of the SHD/DNA Complex and Gel Retardation Assay. To prepare the SHD/DNA complex, 400 ng of DNA was incubated with SHDs in distilled water to form the SHD/DNA complex at 37 °C for 30 min with different R/P ratios (1, 2.5, 5, 10, 15, 20, and 30). The DNA condensation ability of SHDs was assessed by a gel electrophoresis method. These samples were loaded onto 1% (w/v) agarose gel with tris-acetate (TAE) buffer solution and electrophoresed at 100 V for 60 min. DNA in the gel was visualized by GoldView staining, and SHDs in the gel were visualized by their inherent fluorescence. DNA retardation was recorded by a UV illuminator (Bio-Rad ChemiDoc XRS+, USA) and analyzed with Image Lab software. The size and morphology of the SHD/DNA complex were determined by DLS, TEM, SEM, and AFM.

***In Vitro* Gene Transfection.** The HepG2 tumor cell line was cultured in DMEM supplemented with 10% (v/v) heat-inactivated FBS and 1% (v/v) penicillin-streptomycin solution at 37 °C in 5% CO_2. HepG2 cells were seeded in a 96-well plate with an initial density of 1 × 10^4 cells per well and incubated for 24 h. The cells were transfected with the SHD/pGL-3 complex with the R/P ratio at 2.5, 5, 10, 15, and 20. After incubation for 48 h, the medium was removed and the cells were gently washed by PBS. The cells were lysed using 70 μL of luciferase lysis buffer followed by freezing−thawing (−80 °C) cycles. Luciferase activity was detected by the light emission from the 20 μL of cell lysate with 50 μL of luciferase substrate using a Varioskan Flash microplate reader (Thermo Fisher Scientific, USA). The total protein of cell extracts was measured according to a BCA protein assay kit. The relative light units (RLU) were normalized against the total protein, and gene transfection efficiency was presented as RLU/mg protein. The PDs (R/P 20, with (+)FBS), PEI 25k (N/P 10, with (+)FBS), and PEI 25k (N/P 10, without (−)FBS) were used as controls.

***In Vitro* Cytotoxicity.** Cell viability assay and cell apoptosis assay were used to evaluate *in vitro* cytotoxicity of SHDs. HepG2 cells were cultured in a 96-well plate with an initial density of 1 × 10^4 cells per well for 24 h. HepG2 cells were treated with the SHD/DNA complex (R/P 2.5, 5, 10, 15, and 20) and the PEI/DNA complex (N/P 10). After incubation for 48 h, cell viability was quantified by a CCK-8 kit. The absorbance at 450 nm was measured using Varioskan Flash microplate reader. The cells in the culture plate were used as blank controls. The relative cell viability was calculated by the equation: cell viability = $(OD_{sample} - OD_{background})/(OD_{control} - OD_{background}) \times 100\%$.

HepG2 cells were cultured in a 6-well plate with an initial density of 2 × 10^6 cells per well for 24 h. Then HepG2 cells were incubated with the SHD/DNA complex (R/P 20) and the PEI/DNA complex (N/P 10) for 48 h. The cells were harvested and fixed with 70% ethanol at 4 °C for 2 h. The cells were stained by the PI kit for 30 min, and cell apoptosis was quantified by a fluorescence-activated cell sorting (Beckman Coulter Cytomics FC-500, USA) with excitation (ex) at 488 nm and emission (em) at 575 nm. The cells in the culture plate were used as blank controls.

Intracellular Tracking of Gene Delivery. Confocal laser scanning microscopy (Leica TCS SP5, Germany), live cell imaging system (Leica DMI6000B, Germany), and TEM for cell ultrathin sections were used to track intracellular gene delivery of the SHD/pGL3-Luc complex. HepG2 cells were cultured in glass-bottomed dishes with an initial density of 1 × 10^4 cells per well for 24 h. The cells were incubated with the SHD/pGL3-Luc (R/P 20, 300 ng per well of Cy5-labeled pGL3-Luc) complex for 1, 3, 8, and 18 h. Endosomes/lysosomes were stained by LysoTracker Blue DND-22 (75 nM) in DMEM media for 60 min. After the solution was rinsed with PBS, intracellular tracking of the SHD/pGL3-Luc complex could be observed using a CLSM with the SHD channel (red, ex 488 nm and em 605 nm), Cy5-labeled DNA channel (green, ex 633 nm and em 670 nm), LysoTracker-stained endosome/lysosome channel (blue, ex 405 nm and em 422 nm), and light field.

HepG2 cells were cultured in a glass-bottomed dish with an initial density of 1 × 10^4 cells per well for 24 h. The cells were incubated with the complex and observed in real time by a LCIS at 37 °C with 5% CO_2 humidified atmosphere for 1 day. The fluorescence image was acquired every 5 min.

HepG2 cells were cultured in 6-well plates with an initial density of 2 × 10^5 cells per well for 24 h and continued to incubate with the SHD/DNA complex for 24 h. The cells were fixed with 3% glutaraldehyde and 1% osmium tetroxide. After dehydration by acetone, the cells were embedded into

Epon-812 to obtain ultrathin sections, which were doubly stained by lead citrate and uranyl acetate. Subcellular location of the SHD/DNA complex can be observed by a TEM (Hitachi H-600 IV, Japan).

Desired Protein Expression Monitoring. HepG2 cells were cultured in 12-well plates at an initial density of 1×10^5 cells per well for 24 h. To investigate the relationship between SHDs and desired protein expression, different incubating times and different R/P ratios were monitored. On one hand, the cells were incubated with the SHD/pEGFP complex (R/P 20, 2 μg pEGFP) for 2, 12, 24, 36, 48, and 60 h. On the other hand, the cells were incubated with the SHD/pEGFP complex (2 μg pEGFP) at various R/P ratios of 2.5, 5, 10, 15, and 20 for 48 h. After exposure to the SHD/pEGFP complex at designed time points, the cells were washed with PBS three times and harvested. SHD internalization of and GFP expression were quantified by FACS with the SHD channel (ex 488 nm, em FL3) and the GFP channel (ex 488 nm, em FL1).

***In Vivo* Gene Transfection.** All animal experiments were carried out in accordance with the ethics committee of Sichuan Univeristy. To evaluate *in vivo* gene transfection, Balb/c mice and nude mice bearing HepG2 tumor xenografts were administered with the SHD/DNA complex by intramuscular injection or intratumoral injection. The SHD/pCMV-β-gal complex (R/P 20, 10 μg of pCMV-β-gal) or SHD/pGL3-Luc complex (R/P 20, 10 μg of pGL3-Luc) was injected into the tibialis anterior muscles of Balb/c mice. The muscles were harvested at 4 days post-injection to determine the gene transfection efficiency. The β-galactosidase expression was assayed using the β-galactosidase reporter gene assay kit. The gene transfection efficiency was quantified by the luciferase activity as RLU/mg protein. The SHD/pCMV-p53 complex (R/P 20, 20 μg pCMV-p53) was transfected into HepG2 tumor xenografts of nude mice for 2 days. The tumor xenografts were harvested and lysed to extract protein, and total protein was quantified by the BCA assay kit. For Western blot analysis, the equal amount of protein (40 μg) was separated on sodium dodecyl sulfate polyacrylamide gel electrophoresis and transferred onto polyvinylidene fluoride (PVDF) membrane. The PVDF membrane was blocked and incubated with rabbit IgG against human p53 and polyclonal goat anti-rabbit IgG HPR. An enhanced chemiluminescence kit was used to detect the luminescence by a ChemiDoc XRS+UV illuminator (Bio-Rad, USA).

***In Vivo* Fluorescence Imaging.** With injection of the SHD/DNA complex (R/P 20) into muscle or a tumor xenograft, the mice were anesthetized for fluorescence imaging at the monitoring times. Fluorescence signals were detected by an *in vivo* fluorescence imaging system (CRi Maestro EX, USA) with excitation at 450 nm and emission at 605 nm. After administration of the SHD/DNA complex, the fluorescence distribution of organs (heart, liver, spleen, lung, and kidney) were also measured by the fluorescence imaging system.

Conflict of Interest: The authors declare no competing financial interest.

Acknowledgment. This work was supported by National Science Foundation of China (NSFC, Nos. 51133004 and 81361140343), National Basic Research Program of China (National 973 program, No. 2011CB606206), Joint Sino-German Research Project (Nos. GZ756 and GZ905), and the foundation of 2013FZ0003 from the Department of Science and Technology of Sichuan Province.

Supporting Information Available: Materials and methods, experimental details, additional data, and figures (Figures S1−S26). This material is available free of charge *via* the Internet at http://pubs.acs.org.

REFERENCES AND NOTES

1. Peer, D.; Karp, J. M.; Hong, S.; Farokhzad, O. C.; Margalit, R.; Langer, R. Nanocarriers as an Emerging Platform for Cancer Therapy. *Nat. Nanotechnol.* **2007**, *2*, 751–760.
2. Hubbell, J. A.; Chilkoti, A. Nanomaterials for Drug Delivery. *Science* **2012**, *337*, 303–305.
3. Tekade, R. K.; Kumar, P. V.; Jain, N. K. Dendrimers in Oncology: An Expanding Horizon. *Chem. Rev.* **2009**, *109*, 49–87.
4. Lee, C. C.; MacKay, J. A.; Frechet, J. M. J.; Szoka, F. C. Designing Dendrimers for Biological Applications. *Nat. Biotechnol.* **2005**, *23*, 1517–1526.
5. Helms, B.; Meijer, E. W. Dendrimers at Work. *Science* **2006**, *313*, 929–930.
6. Duncan, R.; Izzo, L. Dendrimer Biocompatibility and Toxicity. *Adv. Drug Delivery Rev.* **2005**, *57*, 2215–2237.
7. Liu, H. M.; Wang, H.; Yang, W. J.; Cheng, Y. Y. Disulfide Cross-Linked Low Generation Dendrimers with High Gene Transfection Efficacy, Low Cytotoxicity, and Low Cost. *J. Am. Chem. Soc.* **2012**, *134*, 17680–17687.
8. Huang, C. H.; Nwe, K.; Al Zaki, A.; Brechbiel, M. W.; Tsourkas, A. Biodegradable Polydisulfide Dendrimer Nanoclusters as MRI Contrast Agents. *ACS Nano* **2012**, *6*, 9416–9424.
9. Smith, D. K.; Hirst, A. R.; Love, C. S.; Hardy, J. G.; Brignell, S. V.; Huang, B. Q. Self-Assembly Using Dendritic Building Blocks — Towards Controllable Nanomaterials. *Prog. Polym. Sci.* **2005**, *30*, 220–293.
10. Rosen, B. M.; Wilson, C. J.; Wilson, D. A.; Peterca, M.; Imam, M. R.; Percec, V. Dendron-Mediated Self-Assembly, Disassembly, and Self-Organization of Complex Systems. *Chem. Rev.* **2009**, *109*, 6275–6540.
11. Al-Jamal, K. T.; Ramaswamy, C.; Florence, A. T. Supramolecular Structures from Dendrons and Dendrimers. *Adv. Drug Delivery Rev.* **2005**, *57*, 2238–2270.
12. Shi, J. J.; Votruba, A. R.; Farokhzad, O. C.; Langer, R. Nanotechnology in Drug Delivery and Tissue Engineering: From Discovery to Applications. *Nano Lett.* **2010**, *10*, 3223–3230.
13. Gillies, E. R.; Jonsson, T. B.; Frechet, J. M. J. Stimuli-Responsive Supramolecular Assemblies of Linear-Dendritic Copolymers. *J. Am. Chem. Soc.* **2004**, *126*, 11936–11943.
14. Radowski, M. R.; Shukla, A.; von Berlepsch, H.; Bottcher, C.; Pickaert, G.; Rehage, H.; Haag, R. Supramolecular Aggregates of Dendritic Multishell Architectures as Universal Nanocarriers. *Angew. Chem., Int. Ed.* **2007**, *46*, 1265–1269.
15. Li, Y. P.; Xiao, W. W.; Xiao, K.; Berti, L.; Luo, J. T.; Tseng, H. P.; Fung, G.; Lam, K. S. Well-Defined, Reversible Boronate Crosslinked Nanocarriers for Targeted Drug Delivery in Response to Acidic pH Values and *cis*-Diols. *Angew. Chem., Int. Ed.* **2012**, *51*, 2864–2869.
16. Wood, K. C.; Little, S. R.; Langer, R.; Hammond, P. T. A Family of Hierarchically Self-Assembling Linear-Dendritic Hybrid Polymers for Highly Efficient Targeted Gene Delivery. *Angew. Chem., Int. Ed.* **2005**, *44*, 6704–6708.
17. Barnard, A.; Posocco, P.; Pricl, S.; Calderon, M.; Haag, R.; Hwang, M. E.; Shum, V. W. T.; Pack, D. W.; Smith, D. K. Degradable Self-Assembling Dendrons for Gene Delivery: Experimental and Theoretical Insights into the Barriers to Cellular Uptake. *J. Am. Chem. Soc.* **2011**, *133*, 20288–20300.
18. Yu, T. Z.; Liu, X. X.; Bolcato-Bellemin, A. L.; Wang, Y.; Liu, C.; Erbacher, P.; Qu, F. Q.; Rocchi, P.; Behr, J. P.; Peng, L. An Amphiphilic Dendrimer for Effective Delivery of Small Interfering RNA and Gene Silencing *in Vitro* and *in Vivo*. *Angew. Chem., Int. Ed.* **2012**, *51*, 8478–8484.
19. Skwarczynski, M.; Zaman, M.; Urbani, C. N.; Lin, I. C.; Jia, Z.; Batzloff, M. R.; Good, M. F.; Monteiro, M. J.; Toth, I. Polyacrylate Dendrimer Nanoparticles: A Self-Adjuvanting Vaccine Delivery System. *Angew. Chem., Int. Ed.* **2010**, *49*, 5742–5745.
20. Criscione, J. M.; Le, B. L.; Stern, E.; Brennan, M.; Rahner, C.; Papademetris, X.; Fahmy, T. M. Self-Assembly of pH-Responsive Fluorinated Dendrimer-Based Particulates for Drug Delivery and Noninvasive Imaging. *Biomaterials* **2009**, *30*, 3946–3955.
21. Xu, X. H.; Yuan, H.; Chang, J.; He, B.; Gu, Z. W. Cooperative Hierarchical Self-Assembly of Peptide Dendrimers and Linear Polypeptides into Nanoarchitectures Mimicking Viral Capsids. *Angew. Chem., Int. Ed.* **2012**, *51*, 3130–3133.
22. Xu, X. H.; Li, Y. K.; Li, H. P.; Liu, R.; Sheng, M. M.; He, B.; Gu, Z. W. Smart Nanovehicles Based on pH-Triggered

Disassembly of Supramolecular Peptide-Amphiphiles for Efficient Intracellular Drug Delivery. *Small* **2014**, *10*, 1133–1140.
23. Schaffert, D.; Wagner, E. Gene Therapy Progress and Prospects: Synthetic Polymer-Based Systems. *Gene Ther.* **2008**, *15*, 1131–1138.
24. Petros, R. A.; DeSimone, J. M. Strategies in the Design of Nanoparticles for Therapeutic Applications. *Nat. Rev. Drug Discovery* **2010**, *9*, 615–627.
25. Miyata, K.; Nishiyama, N.; Kataoka, K. Rational Design of Smart Supramolecular Assemblies for Gene Delivery: Chemical Challenges in the Creation of Artificial Viruses. *Chem. Soc. Rev.* **2012**, *41*, 2562–2574.
26. Sanchez, C.; Arribart, H.; Guille, M. M. G. Biomimetism and Bioinspiration as Tools for the Design of Innovative Materials and Systems. *Nat. Mater.* **2005**, *4*, 277–288.
27. Mann, S. Life as a Nanoscale Phenomenon. *Angew. Chem., Int. Ed.* **2008**, *47*, 5306–5320.
28. Wagner, E. Polymers for siRNA Delivery: Inspired by Viruses to be Targeted, Dynamic, and Precise. *Acc. Chem. Res.* **2012**, *45*, 1005–1013.
29. Yoo, J. W.; Irvine, D. J.; Discher, D. E.; Mitragotri, S. Bio-Inspired, Bioengineered and Biomimetic Drug Delivery Carriers. *Nat. Rev. Drug Discovery* **2011**, *10*, 521–535.
30. Sevenson, S.; Tomalia, D. A. Dendrimers in Biomedical Applications: Reflections on the Field. *Adv. Drug Delivery Rev.* **2012**, *64*, 102–115.
31. Mann, S. Self-Assembly and Transformation of Hybrid Nano-objects and Nanostructures under Equilibrium and Non-equilibrium Conditions. *Nat. Mater.* **2009**, *8*, 781–792.
32. Taylor-Pashow, K. M. L.; Della Rocca, J.; Huxford, R. C.; Lin, W. B. Hybrid Nanomaterials for Biomedical Applications. *Chem. Commun.* **2010**, *46*, 5832–5849.
33. Futaki, S. Membrane-Permeable Arginine-Rich Peptides and the Translocation Mechanisms. *Adv. Drug Delivery Rev.* **2005**, *57*, 547–558.
34. Wender, P. A.; Galliher, W. C.; Goun, E. A.; Jones, L. R.; Pillow, T. H. The Design of Guanidinium-Rich Transporters and Their Internalization Mechanisms. *Adv. Drug Delivery Rev.* **2008**, *60*, 452–472.
35. Medintz, I. L.; Uyeda, H. T.; Goldman, E. R.; Mattoussi, H. Quantum Dot Bioconjugates for Imaging, Labelling and Sensing. *Nat. Mater.* **2005**, *4*, 435–446.
36. Ruan, G.; Agrawal, A.; Marcus, A. I.; Nie, S. Imaging and Tracking of Tat Peptide-Conjugated Quantum Dots in Living Cells: New Insights into Nanoparticle Uptake, Intracellular Transport, and Vesicle Shedding. *J. Am. Chem. Soc.* **2007**, *129*, 14759–14766.
37. Tamang, S.; Beaune, G.; Texier, I.; Reiss, P. Aqueous Phase Transfer of InP/ZnS Nanocrystals Conserving Fluorescence and High Colloidal Stability. *ACS Nano* **2011**, *5*, 9392–9402.
38. Palui, G.; Avellini, T.; Zhan, N. Q.; Pan, F.; Gray, D.; Alabugin, I.; Mattoussi, H. Photoinduced Phase Transfer of Luminescent Quantum Dots to Polar and Aqueous Media. *J. Am. Chem. Soc.* **2012**, *134*, 16370–16378.
39. Rybtchinski, B. Adaptive Supramolecular Nanomaterials Based on Strong Noncovalent Interactions. *ACS Nano* **2011**, *5*, 6791–6818.
40. Torchilin, V. P. Multifunctional Nanocarriers. *Adv. Drug Delivery Rev.* **2012**, *64*, 302–315.
41. Gilleron, J.; Querbes, W.; Zeigerer, A.; Borodovsky, A.; Marsico, G.; Schubert, U.; Manygoats, K.; Seifert, S.; Andree, C.; Stoter, M.; *et al.* Image-Based Analysis of Lipid Nanoparticle-Mediated siRNA Delivery, Intracellular Trafficking and Endosomal Escape. *Nat. Biotechnol.* **2013**, *31*, 638–U102.
42. Varkouhi, A. K.; Scholte, M.; Storm, G.; Haisma, H. J. Endosomal Escape Pathways for Delivery of Biologicals. *J. Controlled Release* **2011**, *151*, 220–228.
43. Chang, J.; Xu, X. H.; Li, H. P.; Jian, Y. T.; Wang, G.; He, B.; Gu, Z. W. Components Simulation of Viral Envelope *via* Amino Acid Modified Chitosans for Efficient Nucleic Acid Delivery: *In Vitro* and *In Vivo* Study. *Adv. Funct. Mater.* **2013**, *23*, 2691–2699.
44. Ventura, A.; Kirsch, D. G.; McLaughlin, M. E.; Tuveson, D. A.; Grimm, J.; Lintault, L.; Newman, J.; Reczek, E. E.; Weissleder, R.; Jacks, T. Restoration of p53 Function Leads to Tumour Regression *in Vivo*. *Nature* **2007**, *445*, 661–665.